PCCP

PAPER

View Article Online
View Journal | View Issue

Check for updates

Cite this: *Phys. Chem. Chem. Phys.*, 2026, **28**, 7766

# Rotational dynamics of diammonium cations in lead bromide composites investigated by quasi-elastic neutron scattering

Kanming Shi, [a] Lorenzo Malavasi, [b] Fanni Juranyi[c] and Maths Karlsson *[a]

Received 18th December 2025,
Accepted 17th February 2026

DOI: 10.1039/d5cp04945h

rsc.li/pccp

We report results from quasielastic neutron scattering (QENS) measurements of the dynamical nature of diammonium cations in the two-dimensional (2D) metal halide perovskites (MHPs) (1,3-PDA)$PbBr_4$ (PDA: phenylenediammonium), (1,4-PDA)$PbBr_4$, and (1,4-XDA)$PbBr_4$ (XDA: xylylenediammonium), and in the zero-dimensional (0D) perovskitoid $(1,3\text{-XDA})_2PbBr_6$. QENS spectra measured upon heating from 44 to 350 K reveal the onset of picosecond timescale dynamics of the respective organic cation at around 225 K for 1,3-PDA, 250 K for 1,4-PDA, 250 K for 1,3-XDA, and 350 K for 1,4-XDA. Analyses of the elastic incoherent structure factor of the materials suggest that the observed dynamics can be assigned to three-fold ($C_3$) and/or continuous rotational jump-diffusion dynamics of the terminal $-NH_3$ groups of the respective organic cation for all materials. An average, apparent, residence time of the jump-diffusion dynamics has been extracted from the QENS data and takes values of about 1 ps for (1,3-PDA)$PbBr_4$, 4–5 ps for (1,4-PDA)$PbBr_4$ and $(1,3\text{-XDA})Pb_2Br_6$, and 10 ps for (1,4-XDA)$PbBr_4$ at 350 K. A comparison of the dynamical results with the length and symmetry of the organic cations suggests that a smaller organic cation (here PDA) and an asymmetric position of the two $-NH_3$ groups (here 1,3-PDA and 1,3-XDA) correlate with a lower onset temperature and faster dynamics. A comparison of the dynamics results with the photoluminescence (PL) spectra of the materials may indicate that slower $-NH_3$ dynamics correlates with a lower thermal stability of PL due to less dynamic disorder.

Open Access Article. Published on 11 March 2026. Downloaded on 4/7/2026 5:31:09 PM.
This article is licensed under a Creative Commons Attribution 3.0 Unported Licence.

## 1. Introduction

Layered, or 2D, metal halide perovskites (MHPs)—particularly those of the Ruddlesden–Popper type $A_2A'_{n-1}M_nX_{3n+1}$ and the Dion–Jacobson type $AA'_{n-1}M_nX_{3n+1}$—are attracting considerable interest for optoelectronic applications.[1–4] In these structures, A and A′ are organic cations, and $n$ denotes the number of stacked inorganic layers composed of octahedral $MX_6$ units, where M is a metal cation and X is a halide ion. Amongst the 2D MHPs developed so far, most are based on monoammonium cations, whereas diammonium cations have been less explored.[5–9]

Recently, a new class of Dion–Jacobson type MHPs, with A = 1,3-phenylenediammonium (1,3-PDA, PDA = $C_6H_5(NH_3)_2^{2+}$), 1,4-phenylenediammonium (1,4-PDA), and 1,4-xylylenediammonium (1,4-XDA, XDA = $C_6H_5(CH_2NH_3)_2^{2+}$), M = Pb, and X = Br, as well as the chemically similar but structurally dissimilar material $(1,3\text{-XDA})_2PbBr_6$, were reported.[10] The latter material exhibits isolated octahedral $PbBr_6$ building blocks and may therefore be described as a zero-dimensional (0D) perovskitoid; see Fig. 1 for the crystal structure of each material. While all four materials show PL in the visible wavelength region upon excitation at 300 nm,[10] the nature of the PL varies markedly between the different materials. Specifically, the materials with the relatively short organic cations, (1,3-PDA)$PbBr_4$ and (1,4-PDA)$PbBr_4$, exhibit relatively broad PL in the wavelength range of 450–750 nm, whereas the material with the relatively long organic cation, (1,4-XDA)$PbBr_4$, exhibits a narrower PL in the wavelength range of 400–450 nm;[10] the PL of $(1,3\text{-XDA})_2PbBr_6$ has not yet been reported. Furthermore, the material with the more asymmetric organic cation, (1,3-PDA)$PbBr_4$, generally exhibits a weaker PL compared to (1,4-PDA)$PbBr_4$ and (1,4-XDA)$PbBr_4$, which have been correlated to the degree of distortion of the octahedral $PbBr_6$ building blocks.[10]

In addition to the correlation between the degree of octahedral distortion and PL properties, recent results based on QENS experiments on similar 2D MHPs, such as $(n\text{BA})_2PbBr_4$, (ODA)$PbBr_4$ and $(GABA)_2PbBr_4$, where $n$BA = $n$-butylammonium, ODA = 1,8-diaminooctammonium, and GABA = 4-aminobutyric acid, suggest that the PL properties are affected by the reorientational motions of the organic cations.[11] In particular, it has been argued that the relatively smaller organic cation $n$BA is more

[a] *Department of Chemistry and Chemical Engineering, Chalmers University of Technology, SE-412 96, Göteborg, Sweden. E-mail: maths.karlsson@chalmers.se*
[b] *Department of Chemistry, University of Pavia & INSTM, Viale Taramelli 16, 27100, Pavia, Italy*
[c] *Laboratory for Neutron Scattering and Imaging, PSI Center for Neutron and Muon Sciences, Forschungsstrasse 111, 5232, Villigen, Switzerland*

 This journal is © the Owner Societies 2026

Open Access Article. Published on 11 March 2026. Downloaded on 4/7/2026 5:31:09 PM.
This article is licensed under a Creative Commons Attribution 3.0 Unported Licence.

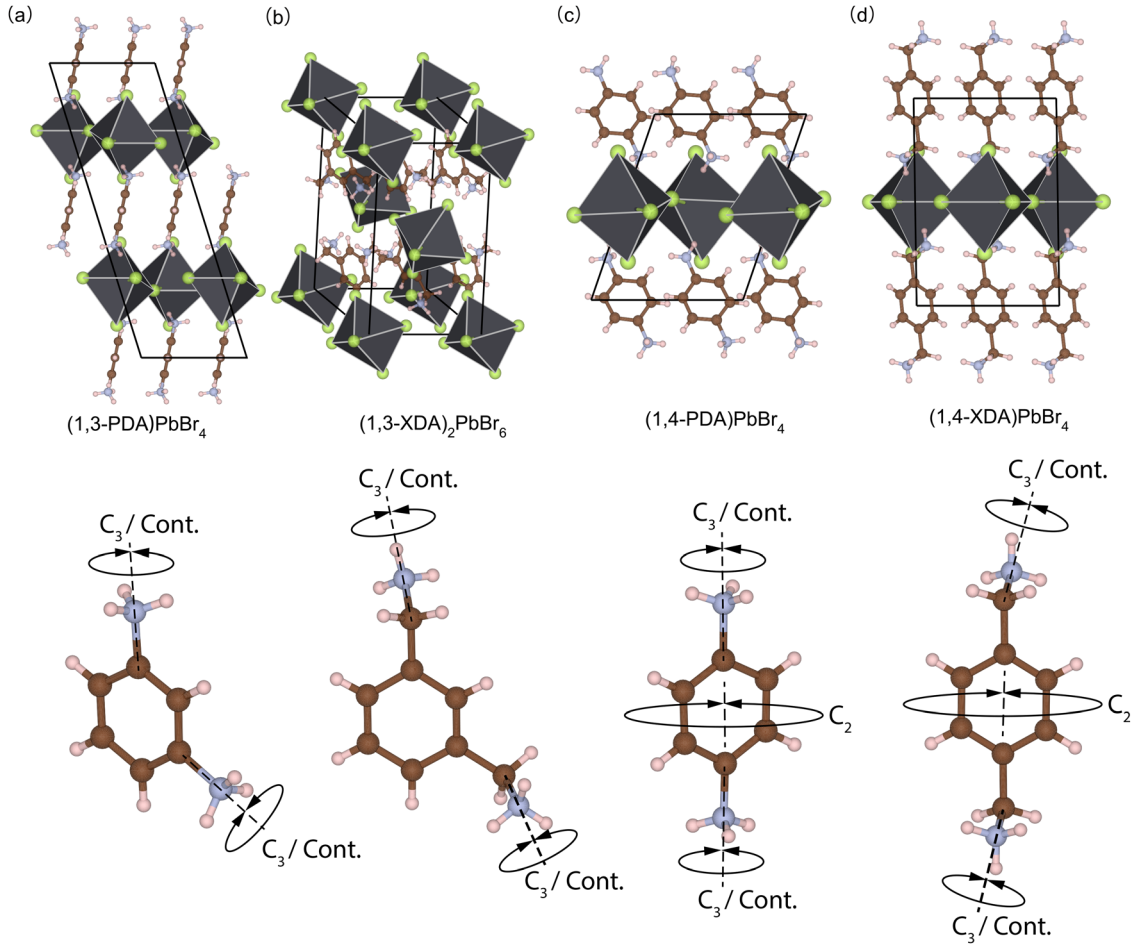


Fig. 1 Illustration of the crystal structures and organic cations of (a) (1,3-PDA)$PbBr_4$ (monoclinic crystal structure with space group $C2/c$), (b) (1,3-XDA)$_2PbBr_6$ (monoclinic crystal structure with space group $P2_1/c$), (c) (1,4-PDA)$PbBr_4$ (triclinic crystal structure with space group $P\bar{1}$), and (d) (1,4-XDA)$PbBr_4$ (monoclinic crystal structure with space group $P2_1/c$), according to ref. 10. The black lines refer to a unit cell. The lower part of the figure illustrates the $C_3$ and continuous (Cont.) rotational diffusion of the terminal $-NH_3$ groups, as well as $C_2$ rotational diffusion of the phenylene group ($-C_6H_4-$) along its long molecular axis for (1,4-PDA)$PbBr_4$ and (1,4-XDA)$PbBr_4$ (see the Results section). Br atoms are indicated as green spheres, C atoms as brown spheres, N atoms as light blue spheres, and H atoms as light pink spheres. The Pb atoms located inside the $PbBr_6$ octahedra are omitted. The crystal structures were plotted using VESTA.[12]

dynamic inside the inorganic sublattice, which gives rise to a larger "dynamic radius", which yields a closer to ideal A-site geometry, preventing local structural distortions and broadband PL.[11]

In this work, we investigate the reorientational dynamics of the organic cations in the novel 2D MHPs (1,3-PDA)$PbBr_4$, (1,4-PDA)$PbBr_4$, and (1,4-XDA)$PbBr_4$, and in the 0D perovskitoid (1,3-XDA)$_2PbBr_6$ using QENS. The aim of this study is to determine the onset temperature and geometry of the dynamics, how it correlates with the materials' PL properties, and how it compares with the organic cation dynamics in other, related, MHPs.

# 2. Experimental

## 2.1. Sample synthesis

Single crystals of (1,3-PDA)$PbBr_4$, (1,4-PDA)$PbBr_4$, (1,3-XDA)$_2PbBr_6$ and (1,4-XDA)$PbBr_4$ were grown by dissolving lead(II) acetate powder in a large excess of 48% w/w aqueous HBr and 50% w/w aqueous $H_3PO_2$, and heating the mixture to 140 °C. After solid dissolution, a stoichiometric amount of solid diamine (liquid for 1,3-XDA) was added. Subsequently, crystals formed upon slow cooling to room temperature. X-ray diffraction data, obtained using a Bruker D8 Discover with a Cu source, and energy-integrated neutron scattering data both confirm phase purity and that the samples adopt the crystal structures previously reported for these materials; see Fig. S1 in the SI.

## 2.2. Quasielastic neutron scattering

The QENS experiment was performed on the direct geometry time-of-flight spectrometer FOCUS at the continuous spallation neutron source SINQ at the Paul Scherrer Institute in Switzerland.[13,14] The samples, approximately 1 g per composition, were contained in an aluminium foil rolled cylinder with an expanded size of 5 cm × 4 cm, which was sealed in an aluminium cylinder can with a lead wire. The instrument was

Open Access Article. Published on 11 March 2026. Downloaded on 4/7/2026 5:31:09 PM. This article is licensed under a Creative Commons Attribution 3.0 Unported Licence.

set up using an incident neutron wavelength ($\lambda_{incident}$) of 4 Å. By using this setting, the energy resolution (determined as the full-width at half maximum (FWHM) of the elastic line) was 0.2 meV, the accessible momentum transfer ($Q$) range was 0.4–2.5 Å$^{-1}$, and the observation time window of the dynamics was ~0.2–13 ps. Measurements were performed at temperatures ($T$) of 44 K, 200 K, 225 K, 250 K, 300 K, and 350 K, in that order. The measurement time at each temperature was approximately 2 h.

The data reduction was performed using the DAVE software.[15] Data from the measurement of an empty sample cell at the same temperatures as those used for the samples were subtracted from the data for the samples, and all data were divided by the data from the measurement of a vanadium standard at 300 K to correct for variations in the efficiency of the different detectors. The measured scattering intensity is proportional to the dynamical structure factor $S(Q, E)$, which results from the sum of coherent and incoherent scattering contributions. The $S(Q, E)$ data were sliced into $Q$ regions of 0.15 Å$^{-1}$ width.

# 3. Results

## 3.1. Dynamical structure factors

Fig. 2 shows the dynamical structure factors, $S(Q, E)$, as integrated over the measured $Q$-range, for temperatures between 200 and 350 K, together with the instrumental resolution function, $R(E)$. The latter is approximated with the spectrum measured at 44 K, where QENS studies of similar materials have shown that the diffusion dynamics of organic cations on the picosecond timescale are frozen-in.[11,17] Note that, for (1,3-PDA)$PbBr_4$ there was a problem in the data collection at 44 K and, therefore, for the analysis of the neutron scattering data for this sample, the 44 K data for (1,3-XDA)$_2PbBr_6$ were used.

Our general observation is that the spectra for $T > 200$ K are markedly different from the spectra of the resolution function.

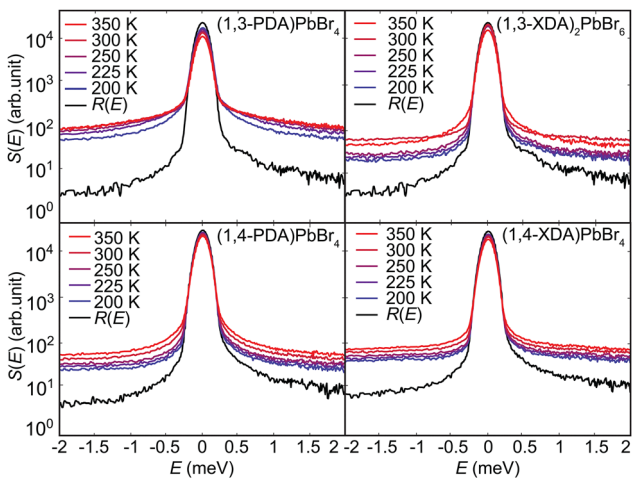


Fig. 2 Variable temperature $Q$-integrated dynamical structure factors, $S(E)$, for the 2D MHPs (1,3-PDA)$PbBr_4$, (1,4-PDA)$PbBr_4$, and (1,4-XDA)$PbBr_4$, and the 0D perovskitoid (1,3-XDA)$_2PbBr_6$.

The onset of quasielastic scattering is observed at approximately 225 K for (1,3-PDA)$PbBr_4$, 250 K for (1,4-PDA)$PbBr_4$, 250 K for (1,3-XDA)$PbBr_6$, and 350 K for (1,4-XDA)$PbBr_4$. In this context, we note that H contributes approximately 90% for (1,3-PDA)$PbBr_4$, 90% for (1,4-PDA)$PbBr_4$, 93% for (1,3-XDA)$_2PbBr_6$, and 92% for (1,4-XDA)$PbBr_4$ to the total scattering cross section of the investigated materials, and H scatters mainly incoherently (*cf.* 80.3 barns for the incoherent scattering cross section and 1.8 barns for the coherent scattering cross section),[16] which suggests that the quasielastic signal originates from the dynamics of the H of the organic cations. As reported in some other QENS studies of MHPs, strongly damped or over-damped vibrational dynamics of the octahedral units of the inorganic sublattice, here $PbBr_6$, can also give rise to significant quasielastic scattering.[18–21] However, such dynamics are usually observed in the vicinity of displacive phase transitions. Given the absence of such phase transitions in the materials studied here, combined with the much smaller contribution from $PbBr_6$ to the total scattering cross section, it is reasonable to assume that the quasielastic signal can be approximated with the self-dynamics of the H of the organic cations.

In our more detailed analysis, $S(Q, E)$ was fitted according to the following function:

$$S(Q,E) = \left[I_{el}\cdot\delta(E) + I_{qe}\cdot\mathcal{L}(E)\right] \otimes R(Q,E) + bkg(Q),$$
$$\mathcal{L}(E) = \frac{1}{\pi}\frac{\gamma}{\gamma^2 + E^2} \quad (1)$$

Here, $I_{el}\cdot\delta(E)$ is the elastic scattering intensity, which accounts for the intensity at zero energy transfer ($E = 0$). In our case, elastic scattering originates from H atoms that can be considered immobile within the observation time window. $I_{qe}\cdot\mathcal{L}(E)$ is a Lorentzian function of amplitude $I_{qe}$ and half-width at half maximum (HWHM) $\gamma$. $\otimes$ denotes the convolution operation, $R(Q, E)$ is the instrumental resolution function, and $bkg(Q)$ is an $E$-independent background. The background relates to (in part) the scattering from phonons, which are centered at energy transfers $\gtrsim 2$ meV (see Fig. 3, which shows $S(E)$ for an extended $E$-range). In comparison, the quasielastic signal typically has a FWHM of less than 1.5 meV, thus not strongly overlapping with the phonon peaks.

Fig. 4 shows, as an example, the fits for $Q = 1.5$ Å$^{-1}$ and $T = 350$ K for all investigated materials, whereas the fits for all temperatures and selected $Q$-values are shown in Fig. S2–S5.

The quasielastic FWHM $\Gamma$ ($\Gamma = 2\gamma$) is (within error) practically $Q$-independent for all materials (Fig. 5), which suggests that the dynamics associated with the quasielastic signal related to organic cation dynamics are localized in nature, in full agreement with other QENS studies of MHPs performed under similar experimental conditions.[17,22] A characteristic timescale ($\tau$) of the dynamics has been derived by taking $\tau = 2\hbar/\bar{\Gamma}$,[23] where $\bar{\Gamma}$ refers to the $Q$-averaged value of $\Gamma$ for each temperature and material. The obtained $\tau$ values are in the range of 1–10 ps and vary significantly between the four samples (Table 1), with the timescale of the dynamics being fastest for (1,3-PDA)$PbBr_4$ (1.2 ps at $T = 350$ K) and slowest for

 This journal is © the Owner Societies 2026

Open Access Article. Published on 11 March 2026. Downloaded on 4/7/2026 5:31:09 PM.
This article is licensed under a Creative Commons Attribution 3.0 Unported Licence.

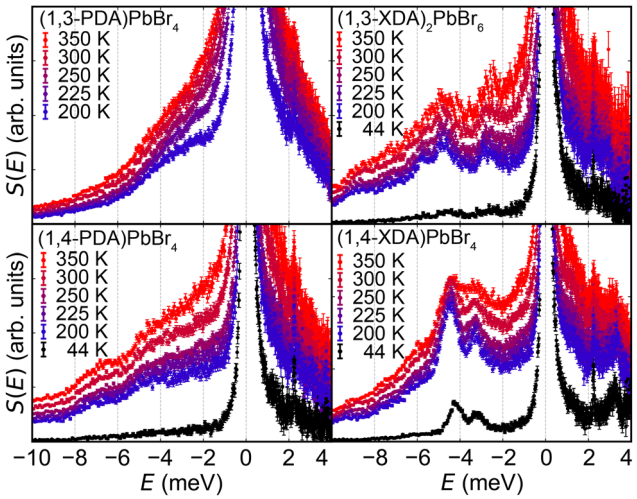


Fig. 3 Variable temperature $Q$-integrated dynamical structure factors, $S(E)$, for the 2D MHPs (1,3-PDA)$PbBr_4$, (1,4-PDA)$PbBr_4$, and (1,4-XDA)$PbBr_4$, and the 0D perovskitoid (1,3-XDA)$_2PbBr_6$, showing the quasielastic and inelastic regions.

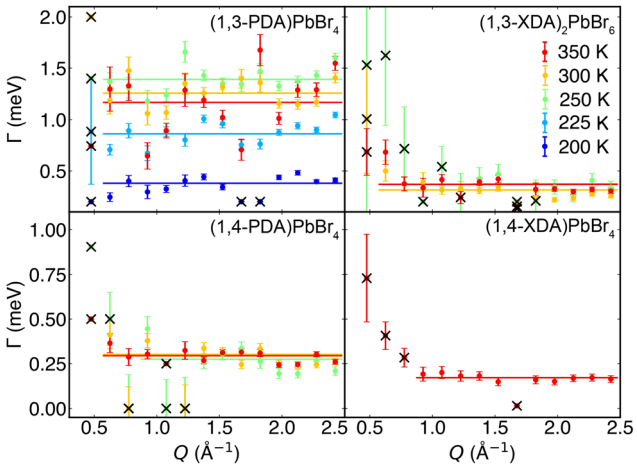


Fig. 5 Quasielastic linewidth $\Gamma$ for the 2D MHPs (1,3-PDA)$PbBr_4$, (1,4-PDA)$PbBr_4$, and (1,4-XDA)$PbBr_4$, and the 0D perovskitoid (1,3-XDA)$_2PbBr_6$. Lines represent fits to a constant at each temperature. The points marked by cross marks are deemed unreliable outliers and are thus excluded from the fits.

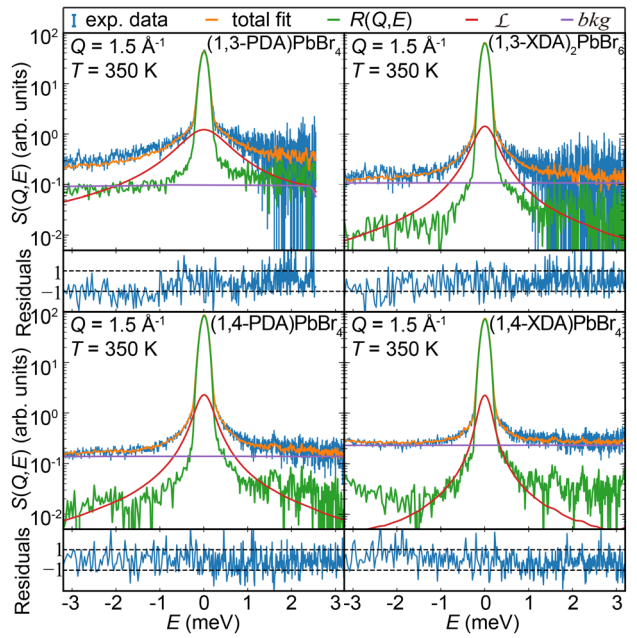


Fig. 4 $S(Q, E)$ for the 2D MHPs (1,3-PDA)$PbBr_4$, (1,4-PDA)$PbBr_4$, and (1,4-XDA)$PbBr_4$, and the 0D perovskitoid (1,3-XDA)$_2PbBr_6$ at $Q$ = 1.5 Å$^{-1}$ and $T$ = 350 K.

(1,4-XDA)$PbBr_4$ (9.5 ps at $T$ = 350 K). Note that the quasielastic signals at $T < 250$ K for (1,4-PDA)$PbBr_4$ and (1,3-XDA)$_2PbBr_6$, and at $T < 350$ K for (1,4-XDA)$PbBr_4$ were too weak to allow a reliable fit according to eqn (1).

### 3.2. Elastic incoherent structure factors

Information about the spatial geometry of the dynamics can be obtained from the analysis of the elastic incoherent structure factor (EISF), which is defined as EISF = $I_{el}/(I_{el} + I_{qe})$. Fig. 6 shows a comparison of the EISF extracted from the experimental data and the EISF model curves for different geometrically and, presumably, physically realistic reorientational motions of the organic cations. For all materials and temperatures, we observe an excellent agreement between the experimental data and the model for three-fold ($C_3$) and continuous (Cont.) rotational diffusion, respectively, of the –$NH_3$ group. These models are mathematically defined as:

$$\mathrm{EISF}_{C3} = c + (1-c)\cdot\frac{1}{n_H}\left[n_H - 6 + 6\cdot\frac{1}{3}(1 + 2\cdot j_0(Qd))\right] \quad (2)$$

$$\mathrm{EISF}_{Cont.} = c + (1-c)\cdot\frac{1}{n_H}\left[n_H - 6 + 6\cdot\frac{1}{N_{max}}\sum_{N=0}^{N_{max}} j_0(Qd_N)\right] \quad (3)$$

Here, $n_H$ is the number of hydrogens in an organic cation, $j_0(x)$ is the zeroth-order spherical Bessel function, $d$ is the jump distance between two hydrogens in an –$NH_3$ group, $N_{max}$ is the number of uniformly distributed jump locations on a circle (theoretically, $N_{max} \to +\infty$, but here we approximate with $N_{max} = 20$), and $d_N = D\sin(N\pi/N_{max})$ is the jump distance between position $N$ and the original position on a circle with diameter $D$. The constant $c$ accounts for additional elastic scattering, probably mostly due to H that experiences motions too slow to be resolved by the instrument resolution, but also to coherent scattering from the materials manifested as peaks in the energy-integrated neutron scattering data (Fig. S1). As can be seen, both models fit equally well to the experimental data and, hence, cannot be distinguished from each other in the relatively limited $Q$-range explored here. Other, geometrically feasible models, such as two-fold ($C_2$) rotation of the whole organic cation around its short molecular axis, or a more complex model that assumes $C_3$ rotation of the –$NH_3$ group together with $C_2$ rotation of the phenylene ring, were also considered; however, all

Open Access Article. Published on 11 March 2026. Downloaded on 4/7/2026 5:31:09 PM.
This article is licensed under a Creative Commons Attribution 3.0 Unported Licence.

Table 1 Compilation of the characteristic timescale, $\tau$, and additional elastic scattering, $c$, values extracted from the QENS data for 2D MHPs (1,3-PDA)$PbBr_4$, (1,4-PDA)$PbBr_4$, and (1,4-XDA)$PbBr_4$, and the 0D perovskitoid (1,3-XDA)$_2PbBr_6$

| | (1,3-PDA)$PbBr_4$ | | (1,3-XDA)$_2PbBr_6$ | | (1,4-PDA)$PbBr_4$ | | (1,4-XDA)$PbBr_4$ | |
|---|---|---|---|---|---|---|---|---|
| $T$ (K) | $\tau$ (ps) | $c$ | $\tau$ (ps) | $c$ | $\tau$ (ps) | $c$ | $\tau$ (ps) | $c$ |
| 200 | 3.3(2) | 0.66(1) | — | — | — | — | — | — |
| 225 | 1.5(1) | 0.55(1) | — | — | — | — | — | — |
| 250 | 0.9(1) | 0.47(1) | 3.7(4) | 0.91(1) | 5.4(5) | 0.91(1) | — | — |
| 300 | 1.1(1) | 0.39(1) | 5.0(3) | 0.71(1) | 4.8(3) | 0.82(1) | — | — |
| 350 | 1.2(1) | 0.25(1) | 4.0(2) | 0.54(1) | 4.7(2) | 0.71(1) | 9.5(10) | 0.63(1) |

of these models showed a worse fit to the data and, hence, were not further considered here (see Fig. S6).

The additional elastic scattering shows a general decrease with increasing temperature, in a quite systematic manner for all materials, which we interpret as an increase in the proportion of organic cations that undergo rotational diffusion of the terminal $-NH_3$ groups within the observation time window; however, it must be noted that for (1,4-PDA)$PbBr_4$ we have data at only one temperature (350 K). Furthermore, a somewhat larger fraction of the organic cations seems mobile in (1,3-XDA)$_2PbBr_6$ and (1,3-PDA)$PbBr_4$, as compared to (1,4-PDA)$PbBr_4$ and (1,4-XDA)$PbBr_4$.

## 4. Discussion

An important result is the observation of picosecond timescale localized dynamics that can be assigned to $C_3$ and/or continuous rotational diffusion of the terminal $-NH_3$ groups of the respective organic cation for all the studied materials. In effect, this means that the spatial geometry of the observed organic cation dynamics is insensitive to the length (here the number of C atoms) and symmetry (here the mutual position of the two $-NH_3$ groups) of the organic cation, as well as to the dimensionality (2D or 0D) of the surrounding inorganic sublattice, for the materials studied here. In contrast, the onset temperature and timescale of the observed dynamics vary significantly amongst the four materials. Firstly, when comparing organic cations of the same length, we find that the asymmetric cations exhibit faster dynamics (*cf.* 1 ps for (1,3-PDA)$PbBr_4$ *vs.* 5 ps for (1,4-PDA)$PbBr_4$, and 4 ps for (1,3-XDA)$_2PbBr_6$ *vs.* 10 ps (1,4-XDA)$PbBr_4$). Secondly, when comparing organic cations of the same symmetry, we find that the shorter cations exhibit a faster timescale of dynamics (*cf.* 1 ps for (1,3-PDA)$PbBr_4$ *vs.* 4 ps for (1,3-XDA)$_2PbBr_6$, and 4 ps for (1,4-PDA)$PbBr_4$ *vs.* 10 ps for (1,4-XDA)$PbBr_4$). Taken together, this suggests that, at a given temperature, a shorter organic cation (here PDA) and an asymmetric position of the two $-NH_3$ groups (here 1,3-PDA and 1,3-XDA) correlate with a lower onset temperature and faster dynamics.

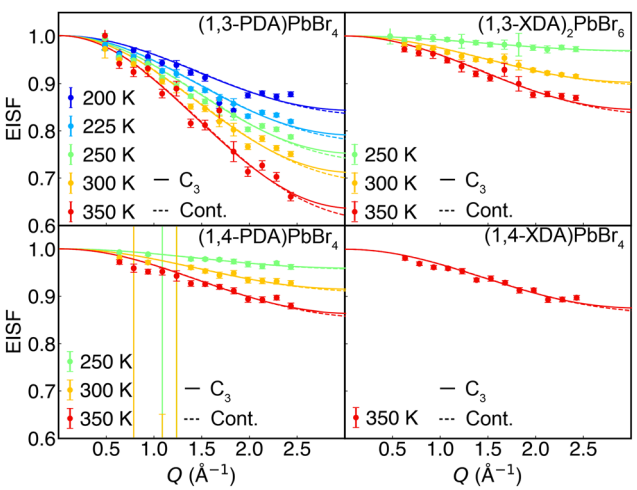


Fig. 6 Experimental EISF (markers) for 2D MHPs (1,3-PDA)$PbBr_4$, (1,4-PDA)$PbBr_4$, and (1,4-XDA)$PbBr_4$, and the 0D perovskitoid (1,3-XDA)$_2PbBr_6$. The solid lines are fits to a $C_3$ jump-diffusion model, and the dashed lines are fits to a model describing continuous diffusion on a circle.

Intuitively, the onset and timescale of the dynamics should be correlated to the strength of the hydrogen-bonding interactions between the $-NH_3$ groups and the surrounding Br atoms of the $PbBr_6$ octahedra, but results from density functional theory (DFT) calculations revealed no systematic differences in the electronic distribution of the investigated materials that would promote the formation of either stronger or weaker hydrogen bonds.[10] Instead, we note that (1,3-PDA)$PbBr_4$ and (1,3-XDA)$Pb_2Br_6$, *i.e.* the materials exhibiting the fastest dynamics, least "immobile" species, and lowest onset temperature of the dynamics, exhibit the largest level of distortion of the $PbBr_6$ octahedral units, whereas the materials exhibiting the slowest dynamics and highest fraction of "immobile" species, (1,4-PDA)$PbBr_4$ and (1,4-XDA)$PbBr_4$, correlate with less octahedral distortion.[10] Additionally, we note that materials having a longer organic cation (XDA) generally exhibit less and slower dynamics compared to their shorter-cation (PDA) counterparts. This feature may be attributed to the additional methylene group ($-CH_2-$) in the longer cations. More specifically, we speculate that the dynamics of the $-CH_2-$ group could take up some thermal energy, which could, possibly, explain that the onset temperature of the dynamics is higher for (1,4-XDA)$PbBr_4$ compared to (1,4-PDA)$PbBr_4$, and for (1,3-XDA)$_2PbBr_6$ compared to (1,3-PDA)$PbBr_4$. Additionally, we note that $C_2$ rotational diffusion of the phenylene group ($-C_6H_4-$) around the long molecular axis may be more readily happening for the more symmetric molecules, 1,4-PDA and 1,4-XDA (see Fig. 1). This may modify the dynamical characteristics of the terminal $-NH_3$ groups, such that some thermal energy is stored in $-C_6H_4-$ dynamics rather than in $-NH_3$ dynamics, thus further increasing its onset temperature.

In comparison to the literature, the observation of $C_3$ and/or continuous rotational dynamics of the $-NH_3$ groups on the picosecond timescale, as observed here, is in agreement with

 This journal is © the Owner Societies 2026

Open Access Article. Published on 11 March 2026. Downloaded on 4/7/2026 5:31:09 PM. This article is licensed under a Creative Commons Attribution 3.0 Unported Licence.

other QENS studies of MHPs, such as $MAPbX_3$ (MA = methylammonium, $CH_3NH_3$; X = I, Br, Cl),[24–27] and 2D $(OA)_2PbI_4$ (OA = $C_8H_{17}NH_3$).[17] However, it is faster than the reported same type of molecular dynamics observed in the 2D MHPs $(n\text{BA})_2PbBr_4$, $(ODA)PbBr_4$ and $(GABA)_2PbBr_4$, for which $C_3$ rotational diffusion of the $-NH_3$ groups was found to occur on a timescale of 30–230 ps at 275–300 K.[11] The slower timescale dynamics compared to our study may be attributed to differences in the observation time window limited by the $E$ range because different instruments were used.

Finally, we compare our dynamical results to the PL properties of the materials. In this context, (1,3-PDA)$PbBr_4$ and (1,4-PDA)$PbBr_4$ exhibit broadband PL (*ca.* 500–900 nm), whereas (1,4-XDA)$PbBr_4$ exhibits narrowband PL at 420 nm together with weaker, broadband PL between 500 and 800 nm.[10] The broadband PL of (1,3-PDA)$PbBr_4$ and (1,4-PDA)$PbBr_4$ has been assigned to radiative relaxation of self-trapped excitons (STEs) due to their more distorted inorganic sublattice and shows a general, systematic decrease in intensity with increasing temperature.[10,28] The broad nature of STE emission in MHPs may also be associated with low-energy, anharmonic phonons due to their generally soft lattices.[20] In this regard, we notice that the phonon peaks for (1,3-PDA)$PbBr_4$ and (1,4-PDA)$PbBr_4$ are broader and have a lower energy compared to (1,4-XDA)$PbBr_4$, for which the phonon peaks are more distinct and exhibit less contribution close to the elastic line (see Fig. 3). The difference in these phonon properties, as well as structural disorder, may thus correlate with the broadness of the PL of the studied materials.

The systematic decrease in the PL intensity with increasing temperature is generally believed to originate from enhanced electron–phonon processes, which depopulate the light-emitting levels in a non-radiative way.[10] However, the softness of the perovskite lattice of MHPs implies that the lattice dynamically reacts to the organic cation dynamics and *vice versa*, and, therefore, the phonons of the inorganic sublattice and the organic cation dynamics are intricately coupled. We speculate that the increase in the portion of mobile $-NH_3$ species, as indicated by the decreasing immobile fraction (*cf.* Table 1) and the concomitant increase in local structural fluctuations (dynamic disorder) induced by transient hydrogen-bonding interactions between the $-NH_3$ groups and the inorganic sublattice, promotes thermal quenching of luminescence. Indeed, previous studies of the 3D MHPs $ABX_3$ (A = Cs, FA, or MA; B = Sn or Pb; X = I, Br, or Cl)[29–31] and the 2D MHP $(C_4H_9NH_3)_2PbBr_4$[32] have shown that dynamic disorder may lead to an increased tendency for non-radiative relaxation through luminescence killer centers. For (1,4-XDA)$PbBr_4$, complexities arising from reabsorption and weak photostability hinder a reliable quantitative analysis of the PL–dynamics relationship.[10] Nevertheless, its comparatively suppressed thermal quenching of luminescence between 77 and 297 K may be related to the relatively slower rotational diffusion of the $-NH_3$ groups in this material compared to the other materials. Therefore, our results may indicate that slower dynamics yields less dynamic disorder and higher thermal stability of PL.

# 5. Conclusions

To conclude, our variable temperature (200–350 K) QENS study of the 2D MHPs (1,3-PDA)$PbBr_4$, (1,4-PDA)$PbBr_4$, (1,4-XDA)$PbBr_4$, and the 0D perovskitoid $(1,3\text{-XDA})_2PbBr_6$ unravelled organic cation dynamics with a characteristic timescale in the range of 1–10 ps that can be attributed to $C_3$ and/or continuous rotational diffusion of the terminal $-NH_3$ groups. The proportion of mobile species generally increases with increasing temperature from 200 to 350 K, and a correlation of the dynamical results with the structural properties of the materials suggests that a smaller organic cation (here PDA) and an asymmetric position of the two $-NH_3$ groups (here 1,3-PDA and 1,3-XDA) correlate with a lower onset temperature and faster dynamics. A comparison of the dynamical results to the PL properties of the investigated materials may indicate a correlation between relatively slow dynamics and little dynamic disorder with high thermal stability of PL; however, it must be noted that the structure–dynamics–PL relationship is likely to be very complex.

# Conflicts of interest

There are no conflicts to declare.

# Data availability

Data for this article, including the neutron scattering data measured at the Paul-Scherrer Institute (PSI), are available in ref. 33.

Supplementary information (SI): energy integrated neutron scattering data, additional $S(Q, E)$ data and fits, and additional EISF models and fits. See DOI: https://doi.org/10.1039/d5cp04945h.

# Acknowledgements

This research was funded by the Swedish Research Council (Grant No. 2016-06958 and 2021-04808) and the Swedish Foundation for Strategic Research within the Swedish National Graduate School in Neutron Scattering, SwedNess (Grant No. GSn15-0008). The authors thank the Paul-Scherrer Institute in Switzerland for access to neutron beam facilities.

# References

1 L. Mao, C. C. Stoumpos and M. G. Kanatzidis, Two-Dimensional Hybrid Halide Perovskites: Principles and Promises, *J. Am. Chem. Soc.*, 2019, **141**, 1171–1190.
2 D. Ghosh, D. Acharya, L. Pedesseau, C. Katan, J. Even, S. Tretiak and A. J. Neukirch, Charge carrier dynamics in two-dimensional hybrid perovskites: Dion–Jacobson vs. Ruddlesden–Popper phases, *J. Mater. Chem. A*, 2020, **8**, 22009–22022.
3 Z. Liu, M. Hu, J. Du, T. Shi, Z. Wang, Z. Zhang, Z. Hu, Z. Zhan, K. Chen, W. Liu, J. Tang, H. Zhang, Y. Leng and

Open Access Article. Published on 11 March 2026. Downloaded on 4/7/2026 5:31:09 PM. This article is licensed under a Creative Commons Attribution 3.0 Unported Licence.

R. Li, Subwavelength-Polarized Quasi-Two-Dimensional Perovskite Single-Mode Nanolaser, *ACS Nano*, 2021, **15**, 6900–6908.

4 Z. Xu, D. Lu, F. Liu, H. Lai, X. Wan, X. Zhang, Y. Liu and Y. Chen, Phase Distribution and Carrier Dynamics in Multiple-Ring Aromatic Spacer-Based Two-Dimensional Ruddlesden–Popper Perovskite Solar Cells, *ACS Nano*, 2020, **14**, 4871–4881.

5 J. Calabrese, N. L. Jones, R. L. Harlow, N. Herron, D. L. Thorn and Y. Wang, Preparation and characterization of layered lead halide compounds, *J. Am. Chem. Soc.*, 1991, **113**, 2328–2330.

6 G. C. Papavassiliou, G. A. Mousdis, C. P. Raptopoulou and A. Terzis, Some New Luminescent Compounds Based on 4-Methylbenzylamine and Lead Halides, *Z. Naturforsch.*, 2000, **55**, 536–540.

7 X. Zhu, N. Mercier, A. Riou, P. Blanchard and P. Frère, $(C_4H_3SCH_2NH_3)_2$ $(CH_3NH_3)Pb_2I_7$: non-centrosymmetrical crystal structure of a bilayer hybrid perovskite, *Chem. Commun.*, 2002, 2160–2161.

8 Y. Li, G. Zheng, C. Lin and J. Lin, Synthesis, structure and optical properties of different dimensional organic–inorganic perovskites, *Solid State Sci.*, 2007, **9**, 855–861.

9 L. Mao, H. Tsai, W. Nie, L. Ma, J. Im, C. C. Stoumpos, C. D. Malliakas, F. Hao, M. R. Wasielewski, A. D. Mohite and M. G. Kanatzidis, Role of Organic Counterion in Lead- and Tin-Based Two-Dimensional Semiconducting Iodide Perovskites and Application in Planar Solar Cells, *Chem. Mater.*, 2016, **28**, 7781–7792.

10 R. Chiara, M. Morana, G. Folpini, A. Olivati, B. Albini, P. Galinetto, L. Chelazzi, S. Ciattini, E. Fantechi, S. A. Serapian, A. Petrozza and L. Malavasi, The templating effect of diammonium cations on the structural and optical properties of lead bromide perovskites: a guide to design broad light emitters, *J. Mater. Chem. C*, 2022, **10**, 12367–12376.

11 A. A. Koegel, E. M. Mozur, I. W. H. Oswald, N. H. Jalarvo, T. R. Prisk, M. Tyagi and J. R. Neilson, Correlating Broadband Photoluminescence with Structural Dynamics in Layered Hybrid Halide Perovskites, *J. Am. Chem. Soc.*, 2022, **144**, 1313–1322.

12 K. Momma and F. Izumi, *VESTA 3* for three-dimensional visualization of crystal, volumetric and morphology data, *J. Appl. Crystallogr.*, 2011, **44**, 1272–1276.

13 S. Janssen, J. Mesot, L. Holitzner, A. Furrer and R. Hempelmann, FOCUS: A hybrid TOF-spectrometer at SINQ, *Physica B*, 1997, **234**, 1174–1176.

14 J. Mesota, S. Janssen, L. Holitzner and R. Hempelmann, FOCUS: Project of a space and time focussing time-of-flight spectrometer for cold neutrons at the Spallation Source SINQ of the Paul Scherrer Institute, *J. Neutron Res.*, 1996, **3**, 293–310.

15 R. T. Azuah, L. R. Kneller, Y. Qiu, P. L. Tregenna-Piggott, C. M. Brown, J. R. Copley and R. M. Dimeo, DAVE: A Comprehensive Software Suite for the Reduction, Visualization, and Analysis of Low Energy Neutron Spectroscopic Data, *J. Res. Natl. Inst. Stand. Technol.*, 2009, **114**, 341–358.

16 web-page: https://www.ncnr.nist.gov/resources/n-lengths.

17 X. Hu, D. Zhang, T. Chen, A. Z. Chen, E. N. Holmgren, Q. Zhang, D. M. Pajerowski, M. Yoon, G. Xu, J. J. Choi and S. H. Lee, Crystal structures and rotational dynamics of a two-dimensional metal halide perovskite $(OA)_2PbI_4$, *J. Chem. Phys.*, 2020, **152**, 014703.

18 Y. Fujii, S. Hoshino, Y. Yamada and G. Shirane, Neutron-scattering study on phase transitions of $CsPbCl_3$, *Phys. Rev. B: Solid State*, 1974, **9**, 4549–4559.

19 T. Lanigan-Atkins, X. He, M. J. Krogstad, D. M. Pajerowski, D. L. Abernathy, G. N. M. N. Xu, Z. Xu, D. Y. Chung, M. G. Kanatzidis, S. Rosenkranz, R. Osborn and O. Delaire, Two-dimensional overdamped fluctuations of the soft perovskite lattice in $CsPbBr_3$, *Nat. Mater.*, 2021, **20**, 977–983.

20 R. Lavén, E. Fransson, P. Erhart, F. Juranyi, G. E. Granroth and M. Karlsson, Unraveling the Nature of Vibrational Dynamics in $CsPbI_3$ by Inelastic Neutron Scattering and Molecular Dynamics Simulations, *J. Phys. Chem. Lett.*, 2025, **16**, 4812–4818.

21 C. Mao, X. He, H.-M. Lin, M. K. Gupta, P. Postec, T. Lanigan-Atkins, M. Krogstad, D. M. Pajerowski, T. Hong, T. J. Williams, J. R. Stewart, D. Y. Chung, M. G. Kanatzidis, S. Rosenkranz, R. Osborn and O. Delaire, Correlated dynamic disorder, octahedral tilts, and acoustic phonon softening in $CsSnBr_3$ and $CsPbBr_3$, *Phys. Rev. Mater.*, 2025, **9**, 065401.

22 A. A. Koegel, I. W. H. Oswald, C. Rivera, S. L. Miller, M. J. Fallon, T. R. Prisk, C. M. Brown and J. R. Neilson, Influence of Inorganic Layer Thickness on Methylammonium Dynamics in Hybrid Perovskite Derivatives, *Chem. Mater.*, 2022, **34**, 8316–8323.

23 R. Hempelmann, *Quasielastic Neutron Scattering and Solid State Diffusion*, Oxford University Press, 2000.

24 T. Chen, B. J. Foley, B. Ipek, M. Tyagi, J. R. Copley, C. M. Brown, J. J. Choi and S. H. Lee, Rotational dynamics of organic cations in the $CH_3NH_3PbI_3$ perovskite, *Phys. Chem. Chem. Phys.*, 2015, **17**, 31278–31286.

25 A. M. Leguy, J. M. Frost, A. P. McMahon, V. G. Sakai, W. Kockelmann, C. Law, X. Li, F. Foglia, A. Walsh, B. C. O'Regan, J. Nelson, J. T. Cabral and P. R. Barnes, The dynamics of methylammonium ions in hybrid organic-inorganic perovskite solar cells, *Nat. Commun.*, 2015, **6**, 7780.

26 I. P. Swainson, C. Stock, S. F. Parker, L. Van Eijck, M. Russina and J. W. Taylor, From soft harmonic phonons to fast relaxational dynamics in $CH_3NH_3PbBr_3$, *Phys. Rev. B: Condens. Matter Mater. Phys.*, 2015, **92**, 100303.

27 G. Schuck, F. Lehmann, J. Ollivier, H. Mutka and S. Schorr, Influence of Chloride Substitution on the Rotational Dynamics of Methylammonium in $MAPbI_{3-x}Cl_x$ Perovskites, *J. Phys. Chem. C*, 2019, **123**, 11436–11446.

28 M. Morana, W. Kaiser, R. Chiara, B. Albini, D. Meggiolaro, E. Mosconi, P. Galinetto, F. De Angelis and L. Malavasi, Origin of Broad Emission Induced by Rigid Aromatic Ditopic Cations in Low-Dimensional Metal Halide Perovskites, *J. Phys. Chem. Lett.*, 2023, **14**, 7860–7868.

 This journal is © the Owner Societies 2026

Open Access Article. Published on 11 March 2026. Downloaded on 4/7/2026 5:31:09 PM.
This article is licensed under a Creative Commons Attribution 3.0 Unported Licence.

29 A. G. Kontos, A. Kaltzoglou, M. K. Arfanis, K. M. McCall, C. C. Stoumpos, B. W. Wessels, P. Falaras and M. G. Kanatzidis, Dynamic Disorder, Band Gap Widening, and Persistent Near-IR Photoluminescence up to At Least 523 K in $ASnI_3$ Perovskites ($A = Cs^+$, $CH_3NH_3^+$ and $NH_2–CH = NH_2^+$), *J. Phys. Chem. C*, 2018, **122**, 26353–26361.
30 M. Baranowski, J. M. Urban, N. Zhang, A. Surrente, D. K. Maude, Z. Andaji-Garmaroudi, S. D. Stranks and P. Plochocka, Static and Dynamic Disorder in Triple-Cation Hybrid Perovskites, *J. Phys. Chem. C*, 2018, **122**, 17473–17480.
31 K. T. Munson and J. B. Asbury, Influence of Dynamic Disorder and Charge–Lattice Interactions on Optoelectronic Properties of Halide Perovskites, *J. Phys. Chem. C*, 2021, **125**, 5427–5435.
32 J. Kang and L.-W. Wang, Dynamic Disorder and Potential Fluctuation in Two-Dimensional Perovskite, *J. Phys. Chem. Lett.*, 2017, **8**, 3875–3880.
33 M. Karlsson, R. Lavén, K. Shi and L. Malavasi, Dynamical properties of novel low-dimensional perovskites for white lighting (PSI), 2022.